CRITICAL DYNAMICS OF BINARY LIQUIDS. RECENT EVIDENCE FROM DYNAMIC LIGHT SCATTERING AND SHEAR VISCOSITY MEASUREMENTS AS WELL AS BROADBAND ULTRASONIC SPECTROMETRY

U. Kaatze, I. Iwanowski

Drittes Physikalisches Institut, Georg-August-Universität, Friedrich-Hund-Platz 1,
37077 Göttingen, Germany, uka@physik3.gwdg.de
(Received 10.05.06)

Ultrasonic attenuation spectra, quasielastic light scattering and shear viscosity measurements of a variety of liquids exhibiting critical fluctuations are discussed. Binary systems without additional relaxation terms in the ultrasonic spectra can be consistently represented by the Bhattacharjee-Ferrell dynamic scaling theory. Results for nonionic surfactant solutions with critical demixing point as well as for phospholipid bilayer systems are presented to indicate couplings between the critical dynamics and noncritical relaxation phenomena.

I. INTRODUCTION

During the past decades much attention has been directed towards the long wavelength fluctuations in the local concentration, associated with the critical demixing of binary fluids. Concentration fluctuations induce anomalies in the thermodynamic parameters as well as the transport properties which largely mask the individual characteristics of the system. The dominant ideas in the theoretical description of such critical phenomena are the "universality", "scaling", and "renormalization" conceptions [1]. Theoretical models, in particular the dynamic scaling [2-6] and the mode-mode coupling [7-12] approaches, have been proposed, including crossover functions describing the transition from the universal Ising-like behaviour to the non-universal mean-field behaviour.

In the experimental verification of theoretical predictions a dominant role is played by static and dynamic light scattering and shear viscosity measurements as well as ultrasonic spectrometry [13,14]. The former methods yield the fluctuation correlation length ξ and the relaxation rate Γ of order parameter fluctuations. Both quantities are related by the dynamic scaling hypothesis [3,15-17]

$$\Gamma = 2D / \xi^2 \tag{1}$$

in which D denotes the mutual diffusion coefficient. The fluctuation correlation length

$$\xi(\in) = \xi_0 \in^{-\tilde{\nu}} \tag{2}$$

and the relaxation rate

$$\Gamma(\in) = \Gamma_0 \in^{Z_0\tilde{\nu}} \tag{3}$$

follow power laws with universal critical exponents $\tilde{\nu}$ and Z_0 and with reduced temperature

$$\in = |T - T_c| / T_c , \tag{4}$$

where T_c denotes the critical temperature. Ultrasonic spectrometry reveals the scaling function $F(\Omega)$ controlling the frequency dependence of the critical contribution to the sonic attenuation coefficient per wavelength

$$\alpha_\lambda^c = Ac_s F(\Omega) \; . \tag{5}$$

Here

$$\Omega = 2\pi\nu / \Gamma(\in) \tag{6}$$

is the scaled (reduced) frequency with ν denoting the frequency itself. Parameter A is an amplitude weakly depending upon ν and c_s is the sound velocity. In Eq. (5)

$$\alpha_\lambda^c = \alpha_\lambda - \alpha_\lambda^b \tag{7}$$

where $\alpha_\lambda = \alpha\lambda$ with α = attenuation coefficient and $\lambda = c_s/\nu$ = wavelength, and with α_λ^b representing the noncritical background part in the attenuation-per-wavelength.

Various theoretical expressions have been presented for the scaling function of critically demixing binary liquids. The three most prominent forms can be empirically represented by the relation [18]

$$F_x(\Omega) = \left[1 + 0.4142(\Omega_{1/2}^x / \Omega)^{n_x}\right]^{-2} \tag{8}$$

with x = BF, FM, and On, where BF indicates the Bhattacharjee-Ferrell dynamic scaling theory [4,5], FM − the Folk-Moser renormalization group theory of the mode-coupling model [11,12], and On − the Onuki intuitive description of the bulk viscosity near the critical point [19,20]. Graphs of these three scaling functions are shown in Fig. 1. The values for the scaled half-attenuation frequency in Eq. (8) are $\Omega_{1/2}^{BF} = 2.1$, $\Omega_{1/2}^{FM} = 3.1$, $\Omega_{1/2}^{On} = 6.2$. The coefficient in the empirical relation takes the values $n_{BF} = 0.5$, $n_{FM} = 0.635$, and $n_{On} = 0.5$ [18].

Because of the different scaling functions following from the theoretical models, a variety of measurements has been performed during the past years in order to verify or disprove the predictions. In this article the results from those measurements of comparatively simple binary mixtures are summarized and used to discuss more complex systems in which, in addition to the fluctuations in the local concentration, further elementary molecular processes occur.
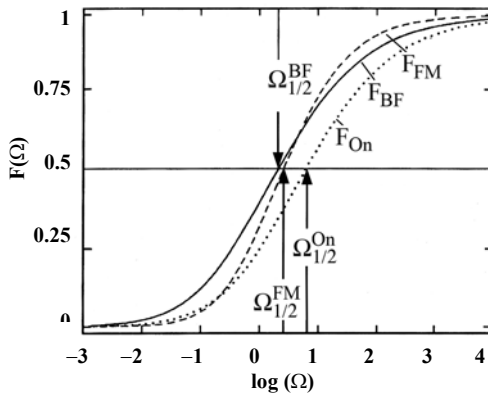
Fig. 1. Graphs of the Bhattacharjee-Ferrell (full line [5]), the Folk-Moser (dashed line [12]), and the Onuki (dotted line [20]) scaling functions. Arrows mark the half-attenuation frequencies.

II. EXPERIMENT

Quasielastic Light Scattering

The mutual diffusion coefficient

$$D = q^{-2}\Gamma_\ell(q,T) \tag{9}$$

of the liquids has been derived from the decay rate $\Gamma_\ell(q,T)$ of the normalized autocorrelation function

$$S_\ell(q,T,t) = \exp[-t\Gamma_\ell(q,T)] \tag{10}$$

of the light quasielastically scattered from the sample. A self-beating digital photon-correlation spectrometer [21,22] has been used for this purpose which was provided with a goniometric system and with a special planar-window cell to enable variations of the scattering angle θ and thus of the wave vector $\vec{q}$ selected by the scattering geometry [23]. The amount of this vector

$$q = \frac{4\pi n}{\lambda_\ell}\sin(\theta/2) \tag{11}$$

depends on the refractive index, measured with the aid of a refractometer (Zeiss, Oberkochen, Germany), and on the wavelength λ_ℓ of the incident light. A frequency-doubled Nd:YAG laser has been used as light source with $\lambda_\ell = 532$ nm. S_ℓ was obtained from a real-time analysis of the scattered light using a digital correlator board (ALV-500/E, Laser, Langen, Germany) which allows for correlation function measurements within a time-scale ranging from 2×10^{-7} s to 3.4×10^3 s [24,25]. The experimental error in the diffusion coefficient values was smaller than 5%. The temperature of the sample was controlled to within ±0.02 K and was measured with an error of less than 0.01 K.

Shear Viscosity

The static shear viscosity of the samples has been measured with a set of Ubbelohde-type capillary viscosimeters (Schott, Mainz, Germany) or with a falling ball viscosimeter (Haake, Karlsruhe, Germany). Both instruments had been calibrated against deionized, distilled and carefully degassed water. The experimental error in these viscosity data was $\Delta\eta_s/\eta_s = 3\%$. Temperature fluctuations during measurements were smaller than ±0.02 K.

Using a shear impedance spectrometer the frequency dependent complex shear viscosity

$$\eta_s(\nu) = \eta_s'(\nu) - i\eta_s''(\nu) \tag{12}$$

of some samples has been measured between 5 MHz and 130 MHz. The method of measurement essentially consists in the determination of the shift in the resonance frequency and of the change in the quality factor of a suitable thickness shear (AT-cut) quartz resonator when the device is loaded with the sample [26]. An example of a complex plane representation of the complex-shear viscosity of a critical mixture [27] is presented in Fig. 2.

Ultrasonic Spectrometry

The acoustical attenuation coefficient α of the mixture has been measured as a function of frequency between 100 kHz and 2 GHz using spot frequency methods. Two different methods have been applied. At low frequencies ($\nu < 15$ MHz) a resonator method has been employed [28-31] which enables α to be determined relative to a suitably chosen reference liquid. At higher frequencies ($\nu > 3$ MHz) absolute measurements of α have been performed applying a pulse-modulated ultrasonic wave transmission method at variable sample thickness [32-36]. Various cells were used, each one matched to a particular frequency range. In Fig. 3, as an example, a spectrum of a mixture of critical composition is shown in the frequency normalized format α/ν^2-vs-ν.
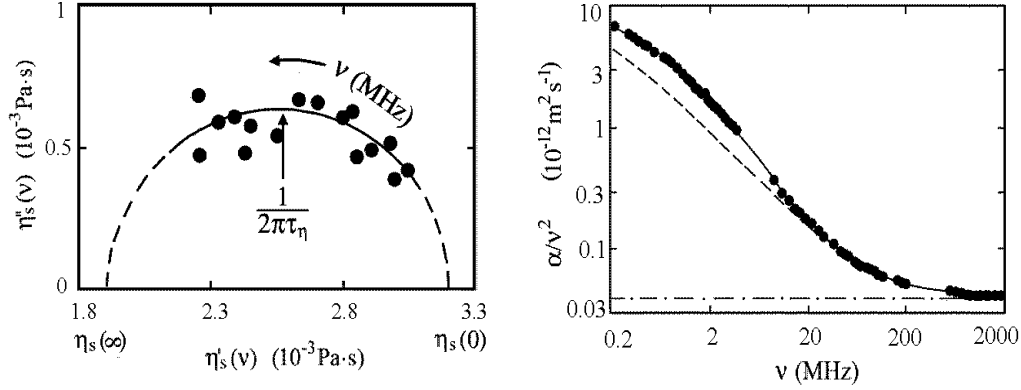
Fig. 2. Complex plane plot of the frequency dependent shear viscosity of the triethylamine-water mixture of critical composition [27] at 291.15 K ($\in$ = 9.2×10^{-4}). The line represents a relaxation spectral function with discrete relaxation time τ_η: $\eta_s(\nu) = \eta_s(\infty) + [\eta_s(0 - \eta_s(\infty)]/[1 + i2\pi\nu\tau_\eta]$.

Fig. 3. Sonic attenuation coefficient per ν^2 versus frequency ν for the triethylene glycol monoheptyl ether/water mixture [37] of critical composition (mass fraction of surfactant $Y = 0.1$) at 288.15 K ($\in$ = 2.8×10^{-2}). The full line represents the model relaxation spectral function representing the experimental data. The dashed line shows the Bhattacharjee-Ferrell term (Eqs. 5, 8) in this function, the dashed-dotted line indicates the frequency independent part $B' = \lim_{\nu\to\infty} (\alpha / \nu^2)$ in the spectrum.

Due to the Bhattacharjee-Ferrell theory the scaling function $F(\Omega)$ can be derived as the ratio [5]

$$F(\Omega) = F^* \alpha_\lambda^c(\nu,T) / \alpha_\lambda^c(\nu,T_c) = F^* \left[\alpha_\lambda(\nu,T) - \alpha_\lambda^b(\nu,T)\right] / \left[\alpha_\lambda(\nu,T_c - \alpha_\lambda^b(\nu,T_c)\right] \quad (13)$$

from the experimental α_λ data where α_λ^b denotes the noncritical background contribution. In relation (13)

$$F^*(T) = \frac{c_s(T_c)A(T_c)}{c_s(T)A(T)} \quad (14)$$

considers the temperature dependence of the sound velocity c_s and the amplitude factor A. Normally $F^* \equiv 1$ is used as originally proposed by Bhattacharjee and Ferrell. Special runs for the determination of the scaling function have been performed with the aid of a plano-concave resonator cell (radius of curvature R_c = 2 m [29]). The focusing action of the concavely shaped end face was utilized in these measurements to reduce unwanted effects from mechanical stress at varying temperature and from small disturbances of the resonator geometry when the sample is exchanged for the reference. An example of several frequency scans of such scaling function measurements is given in Fig. 4.

The temperature of the samples in ultrasonic attenuation coefficient measurements was controlled to within 0.03 K and measured with an error of less than 0.02 K. The error in the attenuation coefficient data was $\Delta\alpha / \alpha$ = 0.05 at $\nu <$ 3 MHz, $\Delta\alpha / \alpha$ = 0.02 at 3 MHz $\le \nu \le$ 50 MHz, and $\Delta\alpha / \alpha$ = 0.01 at 50 MHz $\le \nu \le$ 2 GHz.
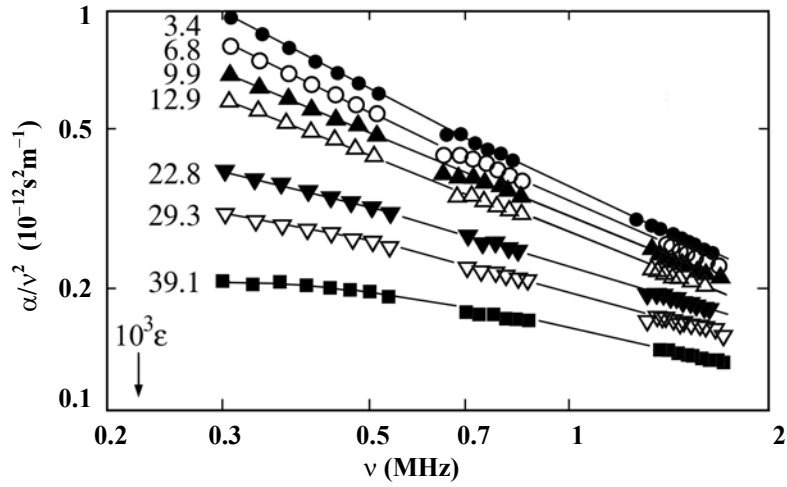
Fig. 4. Low frequency parts of the ultrasonic spectra of the ethanol/dodecane mixture of critical composition (mole fraction of ethanol $X = 0.687$) at some reduced temperatures [38].

III. MIXTURES WITHOUT ADDITIONAL SONIC RELAXATIONS

Relaxation Rate

In Fig. 5 an example is given for the temperature dependence in the shear viscosity of a binary mixture of critical composition. According to the dynamic scaling model, the shear viscosity can be expressed by [40,41]

$$\eta_s(\epsilon) = \eta_b(\epsilon) \exp(Z_\eta H) \tag{15}$$

with the viscosity critical exponent $Z_\eta = 0.065$ [42,43], with the background viscosity

$$\eta_b(\epsilon) = A_\eta \exp[B_\eta /(T - T_\eta)] , \tag{16}$$
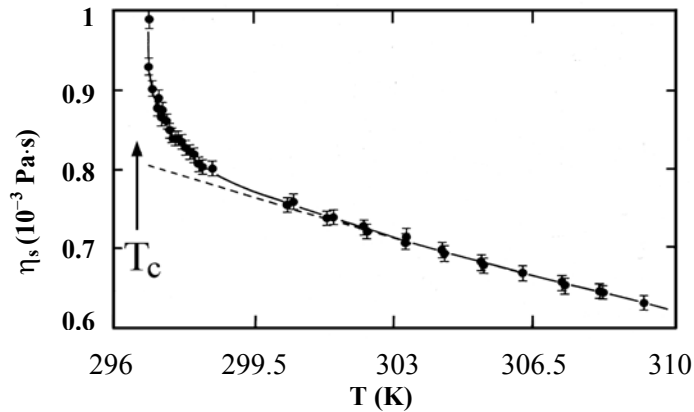
Fig. 5. Shear viscosity η_s, measured with an Ubbelohde capillary and a falling ball viscosimeter, for the nitroethane/cyclohexane mixture of critical composition (mole fraction of nitroethane $X = 0.452$) shown as a function of temperature [39]. The full and dashed lines are graphs of the viscosity function (Eq. 15) and of the background part (Eq. 16), respectively.

and with the crossover function

$$H = H(\xi, q_D, q_c). \tag{17}$$

with the viscosity critical exponent $Z_\eta = 0.065$ [42,43], with the background viscosity

$$\eta_b(\in) = A_\eta \exp[B_\eta /(T - T_\eta)], \tag{16}$$

and with the crossover function

$$H = H(\xi, q_D, q_c). \tag{17}$$

In Eq. (16) parameters A_η, B_η, and T_η are characteristic of the particular mixture under consideration. H, the explicit form of which is given in the literature [40,41,44], depends upon the fluctuation correlation length ξ and on the cut-off wave numbers q_D and q_c. Parameters ξ, q_D, and q_c also control the mutual diffusion coefficient, which likewise consists of a singular part (ΔD) and a background part (D_b) [40,41]

$$D = \Delta D + D_b = \widetilde{D}\left[(1 + b^2 x^2)^{Z_\eta/2} R\Omega_K(x) + \frac{3\pi\eta_s}{16\eta_b}\frac{1+x^2}{\xi}\left(\frac{1}{\widetilde{q}_c} - \frac{1}{q_D}\right)\right] \tag{18}$$

with the Stokes-Einstein-Kawasaki-Ferrell relation [9,17,45,46]

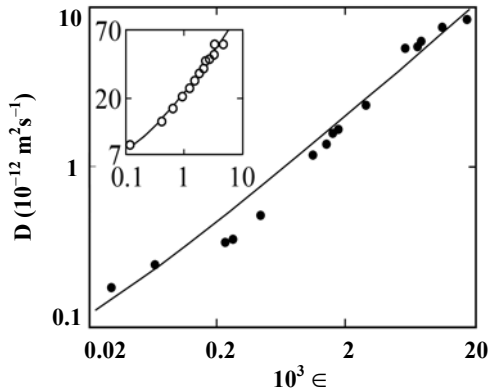$$\widetilde{D} = \frac{k_B T}{6\pi\eta_s\xi} \tag{19}$$

for the diffusion coefficient in the hydrodynamic limit. Here k_B denotes Boltzmann's constant, $x = q\xi$, $b = 0.55$, $R = 1.03$, $\widetilde{q}_c^{-1} = \widetilde{q}_c^{-1} + (2q_D)^{-1}$, and

$$\Omega_K(x) = (3/4x^2)[1 + x^2 + (x^3 - x^{-1})\arctan x] \tag{20}$$

is the Kawasaki function [9].

For two critical mixtures diffusion coefficient data and graphs of Eq. (18) are shown in Fig. 6, indicating that only in the hydrodynamic regime ($q\xi \ll 1$, $\in > 10^{-3}$) the mutual

Fig. 6. Diffusion coefficient D for the nitroethane/3-methylpentane (•[47]) and the nitroethane/cyclohexane (o [39]) mixtures of critical composition shown as a function of reduced temperature $\in$. The lines are graphs of Eq. (18) with parameter values as obtained from the combined evaluation of the dynamic light scattering and shear viscosity data.
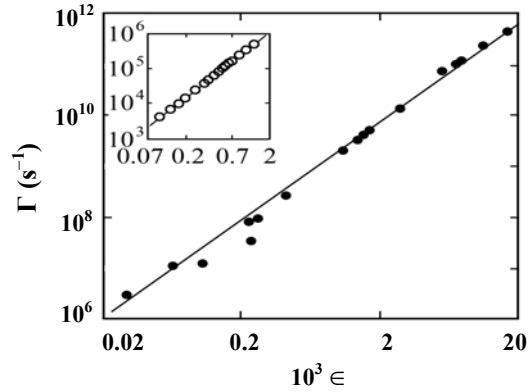
Fig. 7. Relaxation rate Γ of concentration fluctuations for the nitroethane/3-methylpentane (• [47]) and the n-pentanol/nitromethane (o [48]) mixtures of critical composition displayed versus reduced temperature $\in$. The lines represent the power law Eq. (3) with the theoretical values of the exponents and with the amplitudes as given in Table.

diffusion coefficient follows simple power law. Towards the critical temperature D approaches the small but nonvanishing background contribution. Over a significant range of reduced temperatures the relaxation rate follows power law (Eq. 3) with the theoretical critical exponent $Z_0 \tilde{v} = 1.928$. Two examples of experimental Γ-vs-$\in$ relations are given in Fig. 7. For some binary systems the amplitudes ξ_0 and Γ_0, resulting from the combined analysis of shear viscosity and mutual diffusion coefficient data, are collected in Table.

Table. Amplitudes ξ_0 and Γ_0 of the fluctuation correlation length and the relaxation rate, respectively, for some binary critical systems.

Critical mixture	ξ_0, nm	Γ_0, $10^9 \, s^{-1}$
n-pentanol/nitromethane	0.15	187 [48]
nitroethane/cyclohexane	0.16	156 [39]
nitroethane/3-methylpentane	0.23	125 [47]
methanol/*n*-hexane	0.33	44 [49]
methanol/cyclohexane	0.33	26 [50]
ethanol/*n*-dodecane	0.34	8.6 [38]

Scaling Function

In order to calculate the scaling function $F(\Omega)$ of the binary systems listed in Table, a background contribution

$$\alpha_\lambda^b (\nu, T) = B(T)\nu = B'(T)c_s(T)\nu \qquad (21)$$

as resulting from the assumption of a frequency independent high-frequency part (Fig. 3)

$$B'(T) = \lim_{\nu \to \infty}(\alpha / \nu^2) \qquad (22)$$

has been used in Eq. (13). The system methanol/*n*-hexane, however, revealed indications for the existence of a non-critical Debye-type relaxation term [49]. In the spectra of the mixture of critical composition this term appears to be largely masked by the critical part. Therefore, B' has not been taken from an extrapolation according to Eq. (22), but has been treated as an adjustable parameter when fitting experimental $F(\Omega)$ data to the theoretical forms (Eq. 8). Presently, we cannot rule out that hidden contributions from Debye terms exist also in the sonic spectra of other systems, such as ethanol/*n*-dodecane. $F^*(T)$ values different from 1 at $T \neq T_c$, as found with the nitroethane/cyclohexane critical mixture [39], for example, may be taken an indication of an unnoticed hidden relaxation term.

Despite of the open question, whether or not small amplitude relaxation terms are masked by the dominating critical term, the scaling function data derived from the temperature and frequency dependent ultrasonic attenuation coefficients, using the relaxation rates from the quasielectric light scattering and shear viscosity data, nicely fit to the theoretically predicted Bhattacharjee-Ferrell scaling function (Eq. 8 with $x = $ BF). Examples of experimental scaling function data are shown in Fig. 8 where also the graph of the $F_{BF}(\Omega)$ function is given.

Half Attenuation Frequency

The scaled half-attenuation frequency $\Omega_{1/2}^{BF}$ can be derived from the regression analysis of experimental $F(\Omega)$ data in terms of the theoretical scaling function $F_{BF}(\Omega)$. As

$\Omega_{1/2}^{BF}$ has been considered a weak point in the Bhattacharjee-Ferrell model [5] the half-attenuation frequency has been additionally calculated as [53]

$$\Omega_{1/2}^{BF} = \frac{2\pi\nu}{\Gamma(T)}\left[\frac{1}{0.4142}\left(\frac{\alpha_\lambda(T_c) - \alpha_\lambda^b(T_c)}{\alpha_\lambda(T) - \alpha_\lambda^b(T)}\right)^{1/2} - 1\right]^2 . \qquad (23)$$

In these calculations particular weights have been given to the range of small reduced frequencies ($\Omega = 2\pi\nu/\Gamma(T) \leq 10$) where $F_{BF}(\Omega)$ sensitively depends upon $\Omega_{1/2}^{BF}$. Results for two binary critical systems are presented in Fig. 9, indicating $\Omega_{1/2}^{BF} = 2.1 \pm 0.1$. This value is in nice agreement with the theoretical prediction if effects of hydrodynamic coupling are taken into account [5]. The same value resulted also for the methanol/ n-hexane [49] and the methanol/cyclohexane [50] critical mixtures. For the systems n-pentanol/nitromethane ($\Omega_{1/2}^{BF} = 1.8$ [48]) and ethanol/n-dodecane ($\Omega_{1/2}^{BF} = 1.2$ [38]) the half-attenuation frequencies are somewhat smaller. Especially the latter value is likely due to an unnoticed hidden Debye-type relaxation terms.
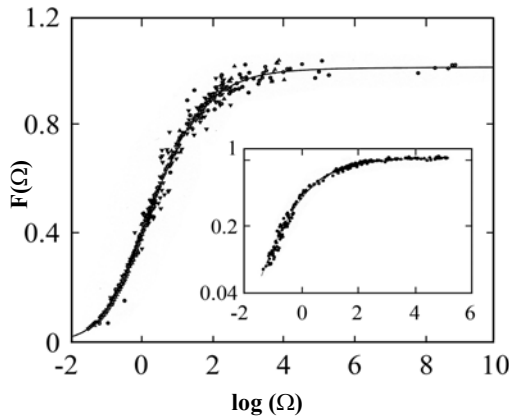
Fig. 8. Scaling function data for the critical systems nitroethane/3-methylpentane (▲ [47]) and nitroethane/cyclohexane (▼ [39]). Points indicate previous data for both systems [51,52]. The inset is a log-log plot of data for the methanol/hexane critical system [49]. Lines are graphs of the Bhattacharjee-Ferrell empirical scaling function (Eq.8 with x = BF).
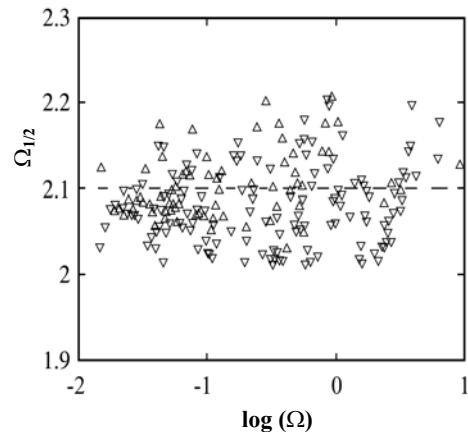
Fig. 9. Scaled half-attenuation frequency data as a function of reduced frequency for the nitroethane/3-methylpentane (Δ [47]) and the nitroethane/cyclohexane (Λ [39]) mixtures of critical composition.

Adiabatic Coupling Constant

According to

$$A(T) = S(T)\nu^{-\delta} \qquad (24)$$

the amplitude parameter A in Eq. (5) is related to the Bhattacharjee-Ferrell amplitude

$$S = \frac{\pi\delta C_{pc}c_s}{2T_c C_{pb}^2}\left[\frac{\Omega_{1/2}^{\mathrm{BF}}\Gamma_0}{2\pi}\right]^{\delta} g^2 . \tag{25}$$

Here

$$\delta = \alpha_0 /(Z_0\tilde{\nu}) = 0.06 \tag{26}$$

with the universal critical exponents Z_0 and $\tilde{\nu}$ and with the specific heat critical exponent α_0. Using Eq. (25) the specific heat is assumed to be given by the simplified version

$$C_p(\in) = C_{pc}\in^{\alpha_0} + C_{pb} \tag{27}$$

of the more general relation [54,55]

$$C_p(\in) = \frac{A^+}{\alpha_0}\in^{-\alpha_0}(1 + D^+\in^{\Delta}) + E\in + B . \tag{28}$$

Parameter g in Eq. (25) denotes the adiabatic coupling constant the amount $|g|$ of which can be calculated from the amplitude S, if the amplitude C_{pc} of the singular part and the background part C_{pb} of the heat capacity are known. For the binary critical systems listed in Table, $|g|$ values between 0.033 (n-pentanol/nitromethane [48]) and 0.26 (nitroethan/3-methylpentan [47]) have been found. These values are small if compared to $|g| = 0.7$ [56] and $|g| = 0.98$ [57] as reported for the triethylamine/water critical mixture or to $|g| = 1.3$ [58] and $|g| = 2.1$ [59] as found for the critical systems ethylammonium nitrate/n-octanol and isobutyric acid/water, respectively. Most of the $|g|$ values derived from the amplitude S of the critical term in the sonic attenuation spectra have been verified using the thermodynamic relation

$$g = \rho(T_c)C_p\left(\frac{dT_c}{dP} - \frac{T\alpha_p}{\rho C_p}\right) \tag{29}$$

in which dT_c/dP denotes the slope in the pressure dependence of the critical temperature and α_p the thermal expansion coefficient at constant pressure. For various critical systems consistency of the results from the shear viscosity, dynamic light scattering, and heat capacity measurements has been additionally shown with the aid of the two-scale factor universality relation [60,61]

$$\xi_0^3 A^+ = k_B X \tag{30}$$

where $X = 0.27$ [4,62,63].

IV. MIXTURES EXHIBITING NONCRITICAL RELATION PHENOMENA

### Nonionic Surfactant Solutions

In addition to the critical term ultrasonic attenuation spectra of many binary systems contain significant contributions from further relaxation terms. An example is the triethylene glycol monoheptyl ether/water (C_7E_3/H_2O) mixture (Fig. 3) the spectra of which reveal contributions exceeding the sum of the high frequency asymptotic background part and the critical part. For another poly(ethylene glycol) monoalkyl ether/water (C_iE_j/H_2O) system a spectrum is shown as excess-attenuation-per-wavelength

$$(\alpha\lambda)_{exc} = \alpha\lambda - B\nu \tag{31}$$

in Fig. 10. In addition to the critical contribution α_λ^c a contribution exists which can be well represented by the restricted version [64]

231
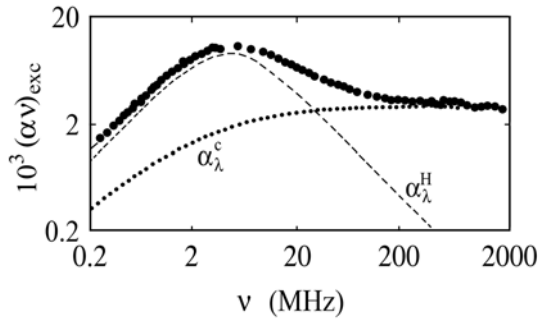
Fig. 10. Ultrasonic excess attenuation spectrum of a C_6E_3/H_2O mixture with surfactant concentration $c = 0.341$ mol/ℓ at 25°C [67]. Dotted and dashed lines indicate the subdivision of the excess spectrum into a Bhattacharjee-Ferrell term α_λ^c (Eq. 5) and a restricted Hill relaxation term α_λ^H (Eq. 32), respectively.
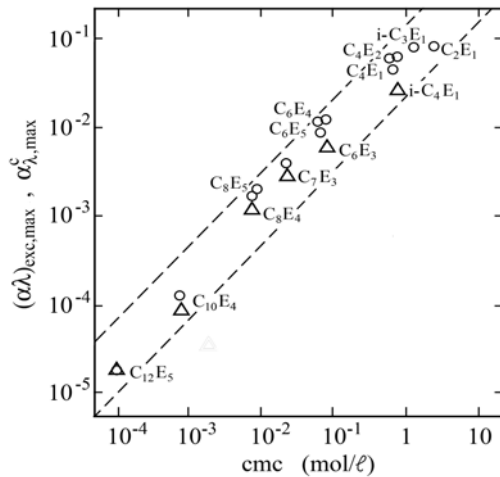
Fig. 11. Maximum values $(\alpha\lambda)_{exc,\max}$ of the excess attenuation spectra (o) and maximum values $\alpha_{\lambda,\max}^c$ of the critical term in the spectra (Δ) for C_iE_j/H_2O mixtures shown as a function of the *cmc* [69,71]. Included in this diagram are also data for short nonionic surfactants [79-81]. Except C_7E_3 (22.5°C) and $C_{10}E_4$ (18°C) the data refer to 25°C.

$$\alpha_\lambda^H = A_H^{\#}\omega\tau_H(1+(\omega\tau_H)^{2s})^{-1/s}$$

(32)

of a Hill relaxation spectral term [65,66]. In this relation $A_H^{\#}$ is the relaxation amplitude, τ_H is the principal relaxation time, and s is a parameter that describes the shape and the width of the underlying relaxation time distribution function. The Hill term is characteristic for all C_iE_j/H_2O mixtures with nonionic surfactant concentration above the critical micelle concentration *cmc* [67-71], except solutions of $C_{12}E_5$ in H_2O for which the *cmc* is very small (10^{-4} mol/ℓ). This feature has suggested the restricted Hill relaxation term to be due to the monomer exchange. It was found [67,68] that the restricted Hill term can be well treated in terms of an extended model [72] of the Teubner - Kahlweit - Aniansson - Wall theory [73-77] of the micelle formation/ decay kinetics. The extension of the theoretical model accounts for the finite width of the relaxation time distribution at surfactant concentrations *c* around the *cmc* and also for the nonlinear dependence of the relaxation time τ_H upon *c* at small concentrations of micellar structures [72].

The focus of interest in various studies of nonionic surfactant solutions with consolute point is the interference of the critical dynamics and the micelle formation/decay kinetics [78]. Interesting, for a large variety of C_iE_j/H_2O systems, covering a *cmc* range from 10^{-4} mol/ℓ up to more than 1 mol/ℓ (Fig. 11) the maximum values $(\alpha\lambda)_{exc,\max}$ of the Bhattacharjee-Ferrell term (Fig. 10) are strongly correlated with the critical micelle concentration. It has thus been concluded that, near the critical demixing point, the micelle formation/decay mechanisms and the critical dynamics of the nonionic surfactant/water mixtures are coupled. Approaching the critical

point the diffusion controlled local fluctuations in the spatial distribution of the micelles, accompanied by local fluctuations in the concentration of monomers appear to act a noticeable influence on the molecular dynamics. Through the rate equations and the law of mass action the micelle formation/decay kinetics is thus governed by the critical or precritical fluctuations in the local micelle concentration [69,71].

V. LIPID MEMBRANES

Critical phenomena are also observed in phospholipid bilayer vesicle solutions. Lipid bilayers are widely accepted models simulating many aspects of biomembrane organization and functions [82-86]. On variation of temperature lipid bilayers pass through a phase transition. At temperatures below the phase transition temperature T_m the membrane exists in a "gel" state in which the hydrocarbon chains of the amphiphilic molecules are stretched and arranged in a rather ordered structure (Fig. 12). At temperatures above T_m the chains are molten and exhibit a significant concentration of rotational isomers. In addition, the arrangement of the lipid molecules in the bilayer membrane is less regular so that the membrane is considered "fluid". Near the phase transition temperature membranes feature a rapidly fluctuating domain structure (Fig. 12). This structure modulates laterally the properties and functions of membranes and is thus assumed essential for living systems [87-89].

The domain sizes cover wide ranges of length scales, extending from molecular dimensions to mesoscopic scales. Since the fluctuations of domains are accompanied by volume and enthalpy fluctuations they couple to sonic fields and can thus be studied by ultrasonic spectroscopy. An example of an ultrasonic excess attenuation spectrum of a phospholipid bilayer solution is displayed in Fig. 13. In addition to a broad critical contribution α_λ^c, two Debye-type relaxation terms α_λ^{D1}, α_λ^{D2} are indicated by relative
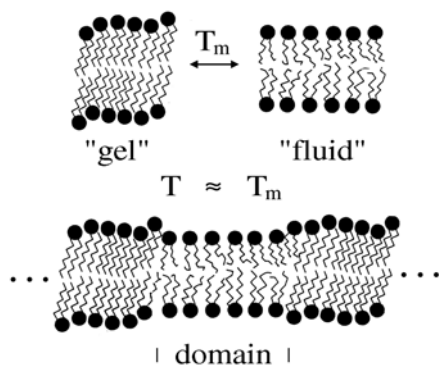
Fig. 12. Structure of phospholipid bilayer membranes below and above the main phase transition temperature T_m (top) and domain structure of the membranes at temperatures around T_m (bottom).
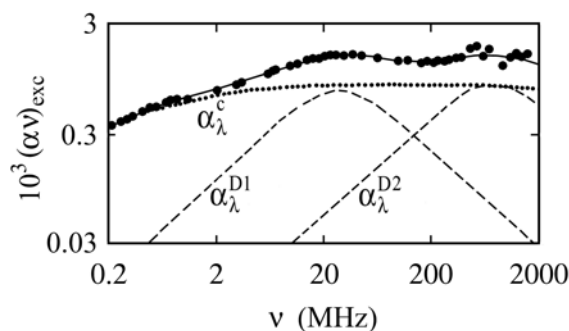
Fig. 13. Ultrasonic excess attenuation-per-wavelength spectrum of an aqueous solution of 1,2-dimyristol-L-3-phosphatidylcholine vesicles (lipid concentration 10 mg/mℓ, 28°C). The subdivision of the spectrum into a Bhattacharjee-Ferrell term (α_λ^c) and two Debye relaxation terms ($\alpha_\lambda^{D1}, \alpha_\lambda^{D2}$) is indicated by dotted and dashed lines, respectively [90,91].

233

maxima in the spectrum of the solution of 1,2-dimyristoyl-L-3-phosphatidylcholine (DMPC) in water [90,91]. These terms can be analytically represented as

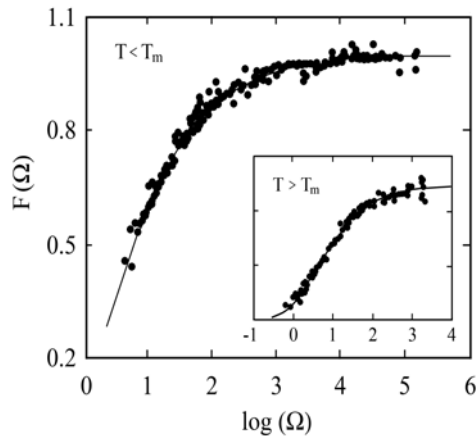$$\alpha_\lambda^{Dj} = \frac{A_{D_j}\omega\tau_{D_j}}{1+\omega^2\tau_{D_j}^2} \tag{33}$$

where j = 1, 2. Empirically the critical contribution can be well represented by the Bhattacharjee-Ferrell spectral function defined by Eq. (5). We mention that the empirical scaling function defined by Eq. (8) and shown in Fig. 1 allows indeed for an appropriate representation of the empirical spectral. In the final evaluation of the measured data, however, the alternative function [92]

$$F_{\mathrm{BF}*}(\Omega) = (2/\Omega)^{1/2}[(1+\Omega^2)^{1/4}\cos(0.5\tan^{-1}\Omega)-1] \tag{34}$$

has been used which had been more recently applied to the critical ultrasonic attenuation near the isotropic-pneumatic-transition of liquid crystals [92].

It is worth to notice that, contrary to concentration fluctuations in critical binary fluids, the Bhattacharjee-Ferrell theory is applied here to the diffusion of the state (gel, fluid) of membrane areas rather than to the diffusion of masses. Another interesting feature of the results for bilayer systems is the finding of the Bhattacharjee-Ferrell theory, originally derived for fully three-dimensional systems, to also hold for quasi-two-dimensional membranes. It has been derived from theoretical arguments [90] that, because the variations in the lateral area of lipid molecules are accompanied by changes in the local thickness of the membrane, the Bhattacharjee-Ferrell model applies well to the domain structure fluctuations. A further noticeable aspect of membrane systems is the possibility to approach the critical temperature T_m from both sides, looking for fluid domains in a gel matrix at $T < T_m$ and for gel like domains in a fluid bilayer at $T > T_m$. Scaling function data for a DMPC/water mixture below and above the gel-fluid phase transition temperature are shown in Fig. 14.

The experimental $F(\Omega)$ data of bilayer membrane systems have been fitted to the scaling function $F_{\mathrm{BF}*}(\Omega)$ treating the relaxation rate Γ of order parameter fluctuations as an adjustable parameter. For a DMPC vesicle solution the relaxation times $\tau_\xi = \Gamma^{-1}$ following thereby are displayed as a function of temperature in Fig. 15. Within the limits of experimental error the relaxation rate data follow power law Eq. (3) with rather small amplitudes ($\Gamma_0 = 1.2\times10^{-9}\,\mathrm{s}^{-1}$, DMPC, $T > T_m$). According to Eq. (1) fluctuation correlation lengths ξ on the order of 10 nm follow from the relaxation rates

Fig. 14. Normalized ultrasonic attenuation coefficient per wavelength, excluding noncritical background contributions for a DMPC vesicle solution in water (lipid concentration 10 mg/m ℓ) at $T < T_m$ and $T > T_m$ (inset) displayed as a function of reduced frequency Ω. Lines are graphs of the scaling function defined by Eq. (34).
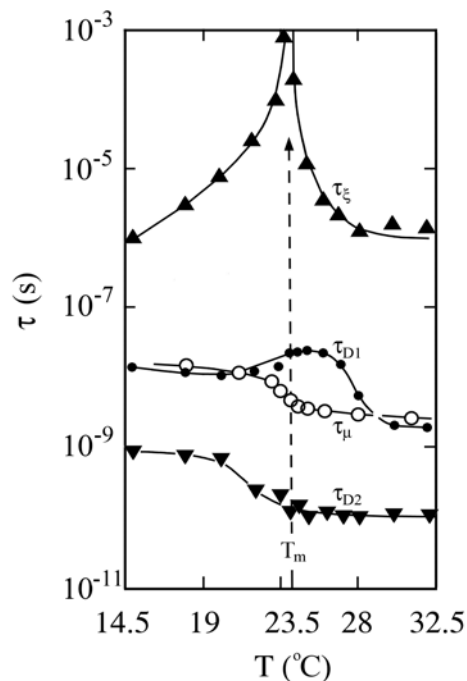
near T_m if diffusion coefficients $D = 3 \times 10^{-11}$ cm^{2}s^{-1} at $T < T_m$ and $D = 7 \times 10^{-9}$ cm^{2}s^{-1} at $T > T_m$ [93] are used.

Also displayed in Fig. 15 are the relaxation times τ_{D1} and τ_{D2} of the Debye-type relaxation terms in the ultrasonic spectra and the dielectric relaxation time τ_μ that characterizes the reorientational motions of the dipolar lipid head groups [94]. The finding that τ_{D1} almost agrees with τ_μ at the same temperature has lead to the conclusion that the low frequency Debye term reflects the axial diffusion of lipids and that, outside the transition region around T_m, the rotation of the molecules and the reorientations of the head groups are coupled. Near T_m the axial diffusion of the molecules slows down whereas the dielectric relaxation displays a stepwise change, indicating significantly faster head group motions at T above T_m than below. The relaxation time τ_{D2} of the high-frequency Debye term coincides with the correlation times of end group (10^{-11} s $- 10^{-10}$ s [95]) and of segmental motions of middle parts (10^{-9} s [95]) of the hydrocarbon lipid chains within the membranes. It also corresponds with the relaxation times of ultrasonic and shear viscosity spectra [96] of liquid n-alkanes of similar chain length.

Fig. 15. Relaxation times of DMPC vesicle solutions as a function of temperature around the gel-fluid phase transition temperature T_m [91].

The high-frequency Debye-type relaxation has thus been assigned to a collective mode of isomerization of the hydrocarbon chains within the lipid bilayer. According to our expectations the chain isomerizations do not slow down at T_m but fasten stepwisely when the lateral area per lipid molecule increases on passing the transition temperature.

VI. CONCLUSIONS

In the homogeneous region near a consolute point the critical dynamics of binary liquid mixtures without additional sonic relaxations can be consistently represented by the Bhattacharjee-Ferrell dynamic scaling model. Ultrasonic spectra can be well described using the relaxation rate as derived from quasielastic light scattering and shear viscosity measurements. If the amplitude of the spectra is treated as an adjustable parameter, the adiabatic coupling constant calculated from its value, additionally using heat-capacity data, within the limits of experimental error agrees with the value derived from an alternative thermodynamic relation.

Use of the Bhattacharjee-Ferrell model for the analytical representation of the critical part in the ultrasonic attenuation spectra or more complicated systems allows for a

favourable description of further relaxation terms. Solutions of nonionic surfactants in water indicate a coupling between the critical dynamics and the micelle formation/decay kinetics. A fluctuation controlled monomer exchange process has been proposed. Near the gel-fluid phase transition ultrasonic spectra of phospholipid bilayer vesicle solutions comprise a critical term which is due to the domain structure fluctuations of the membranes. It can be likewise represented by the Bhattacharjee-Ferrell dynamic scaling theory. Additional Debye-type relaxation terms in the spectra reflect the axial diffusion of the lipid molecules and the structural isomerization of their hydrocarbon chains. The former motions slow near the phase transition temperature, whereas the chain isomerizations are unaffected by the critical dynamics but dependent upon the available lateral area per lipid molecule.

ACKNOWLEDGEMENTS

REFERENCES

1. H.E. Stanley, Rev. Mod. Phys. **71,** 5358 (1999).
2. B.I. Halperin, P.C. Hohenberg, and S. Ma, Phys. Rev. Lett. **29**, 1548 (1972).
3. P.C. Hohenberg and B.I. Halperin, Rev. Mod. Phys. **49**, 435 (1977).
4. J.K. Bhattacharjee and R.A. Ferrell, Phys. Rev. A **24**, 1643 (1981).
5. R.A. Ferrell and J.K. Bhattacharjee, Phys. Rev. A **31**, 1788 (1985).
6. J.K. Bhattacharjee and R.A. Ferrell, Phys. Rev. E **58**, 6246 (1998).
7. M. Fixman, J. Chem. Phys. **36**, 310 (1962).
8. L.P. Kadanoff and J. Swift, Phys. Rev. **165**, 310 (1968).
9. K. Kawasaki, Ann. Phys. (N.Y.) **61**, 1 (1970).
10. K. Kawasaki, Phys. Rev. A **1**, 1750 (1970).
11. R. Folk and G. Moser, Phys. Rev. E **57**, 705 (1998).
12. R. Folk and G. Moser, Phys. Rev. E **58**, 6246 (1998).
13. M.A. Anisimov. Critical Phenomena in Liquids and Liquid Crystals (Gordon and Breach, London, 1991).
14. A. Onuki. Phase Transition Dynamics (Cambridge University Press, Cambridge, 2002).
15. L.P. Kadanoff and J. Swift, Phys. Rev. **166**, 89 (1968).
16. B.I. Halperin and P.C. Hohenberg, Phys. Rev. **177**, 952 (1969).
17. R.A. Ferrell, Phys. Rev. Lett. **24**, 1169 (1970).
18. R. Behrends and U. Kaatze, Europhys. Lett. **65**, 221 (2004).
19. A. Onuki, J. Phys. Soc. Jpn. **66**, 511 (1997).
20. A. Onuki, Phys. Rev. E **55**, 403 (1997).
21. B. Chu. Laser Light Scattering (Academic, New York, 1991).
22. U. Dürr, S.Z. Mirzaev, and U. Kaatze, J. Phys. Chem. A **104**, 8855 (2000).
23. C. Trachimow, L. De Maeyer, and U. Kaatze, J. Phys. Chem. B **102**, 4483 (1998).
24. K. Schatzel, Appl. Phys. B **42**, 193 (1987).
25. K. Schätzel, M. Drewel, and M. Stimac, Mod. Opt. **35**, 711 (1988).
26. R. Behrends and U. Kaatze, Meas. Sci. Technol. **12**, 519 (2001).
27. R. Behrends and U. Kaatze, Phys. Rev. E **68**, 011205 (2003).
28. U. Kaatze, R. Wehrmann, and R. Pottel, J. Phys. E: Sci. Instrum. **20**, 1025 (1987).
29. F. Eggers, U. Kaatze, K.H. Richmann, and T. Telgmann, Meas. Sci. Technol. **5,** 1131 (1994).
30. F. Eggers and U. Kaatze, Meas. Sci. Technol. **7**, 1 (1996).
31. R. Polacek and U. Kaatze, Meas. Sci. Technol. **14**, 1068 (2003).

32. U. Kaatze, K. Lautscham, and M. Brai, J. Phys. E: Sci. Instrum. **21**, 98 (1988).
33. U. Kaatze and K. Lautscham, J. Phys. E: Sci. Instrum. **21**, 402 (1988).
34. U. Kaatze, V. Kühnel, K. Menzel, and S. Schwerdtfeger, Meas. Sci. Technol. **4**, 1257 (1993).
35. U. Kaatze, V. Kühnel, and G. Weiss, Ultrasonics **34**, 51 (1996).
36. U. Kaatze, R. Behrends, and K. Lautscham, Ultrasonics **39**, 393 (2001).
37. J. Haller, R. Behrends, and U. Kaatze, J. Chem. Phys., in press.
38. S.Z. Mirzaev, T. Telgmann, and U. Kaatze, Phys. Rev. E **61**, 542 (2000).
39. R. Behrends, I. Iwanowski, M. Kosmowska, A. Szala, and U. Kaatze, J. Chem. Phys. **121**, 5929 (2004).
40. H.C. Burstyn, J.V. Sengers, J.K. Bhattacharjee, and R.A. Ferrell, Phys. Rev. A **28**, 1567 (1984).
41. R.I. Berg and M.R. Moldover, J. Chem. Phys. **89**, 3694 (1988).
42. J.C.M. Sorensen, R.C. Mockler, and W. O'Sullivan, Phys. Rev. A **16**, 365 (1977).
43. J.C. Nienwouldt and J.V. Sengers, J. Chem. Phys. **90**, 457 (1989).
44. J.K. Bhattacharjee, R.A. Ferrell, R.S. Basu, and J.V. Sengers, Phys. Rev. A **24**, 1469 (1981).
45. G.G. Stokes, Trans. Camb. Phil. Soc. **8**, 287 (1845).
46. A. Einstein, Ann. Physik **17**, 549 (1905).
47. I. Iwanowski, K. Leluk, M. Rudowski, and U. Kaatze, J. Phys. Chem., in press.
48. I. Iwanowski, R. Behrends, and U. Kaatze, J. Chem. Phys. **120**, 9192 (2004).
49. I. Iwanowski, A. Sattarow, R. Behrends, S.Z. Mirzaev, and U. Kaatze, J. Chem. Phys., in press.
50. R. Behrends, U. Kaatze, and M. Schach, J. Chem. Phys. **119**, 7957 (2003).
51. G. Sanchez and C.W. Garland, J. Chem. Phys. **79**, 3090 (1983).
52. G. Sanchez and C.W. Garland, J. Chem. Phys. **79**, 3100 (1983).
53. R. Behrends and U. Kaatze, Europhys. Lett. **65**, 221 (2004).
54. A.C. Flewelling, R.J. DeFonseka, N. Khaleeli, J. Parke, and D.T. Jacobs, J. Chem. Phys. **104**, 8048 (1996).
55. C.A. Cerdeiriña, J. Troncoso, E. Carballo, and L. Romaní, Phys. Rev. E **66**, 031507 (2002).
56. C.W. Garland and C.N. Lai, J. Chem. Phys. **69**, 1342 (1978).
57. R. Behrends, T. Telgmann, and U. Kaatze, J. Chem. Phys. **117**, 9828 (2002).
58. S.Z. Mirzaev and U. Kaatze, Phys. Rev. E **65**, 021509 (2002).
59. U. Kaatze and S.Z. Mirzaev, J. Phys. Chem. **104**, 5430 (2000).
60. A.J. Lui and M.E. Fisher, Physica A **156**, 35 (1989).
61. P.F. Rebillot and D.T. Jacobs, J. Chem. Phys. **109**, 4009 (1998).
62. E.A. Clerke, J.V. Sengers, R.A. Ferrell, and J.K. Bhattacharjee, Phys. Rev. A **27**, 2140 (1983).
63. C. Bervillier and C. Godrèche, Phys. Rev. B **21**, 5427 (1980).
64. K. Menzel, A. Rupprecht, and U. Kaatze, J. Acoust. Soc. Am. **104**, 2741 (1998).
65. R.M. Hill, Nature **275**, 96 (1978).
66. R.M. Hill, Phys. Status Solidi B **103**, 319 (1981).
67. T. Telgmann and U. Kaatze, J. Phys. Chem. A **104**, 1085 (2000).
68. T. Telgmann and U. Kaatze, J. Phys. Chem. A **104**, 4846 (2000).
69. T. Telgmann and U. Kaatze, Langmuir **18**, 3068 (2002).
70. U. Kaatze, Uzbek J. Phys. **5,** 75 (2003).
71. E. Hanke, T. Telgmann, and U. Kaatze, Tenside, Surf. Det. **42**, 7 (2005).
72. T. Telgmann and U. Kaatze, J. Phys. Chem. B **101,** 7766 (1997).
73. M. Teubner, J. Phys. Chem. **83**, 2917 (1979).
74. M. Kahlweit and M. Teubner, Adv. Colloid Interface Sci. **13**, 1 (1980).
75. E.A.G. Aniansson and S.N. Wall, J. Phys. Chem. **78**, 1024 (1974).
76. E.A.G. Aniansson and S.N. Wall, J. Phys. Chem. **79**, 857 (1975).
77. E.A.G. Aniansson, Progr. Colloid Polym. Sci. **70**, 2 (1985).
78. A. Zielesny, L. Belkoura, and D. Woermann, Ber. Bunsenges. Phys. Chem. **98**, 579 (1994).

79. K. Menzel, A. Rupprecht, and U. Kaatze, J. Phys. Chem. B **101**, 1255 (1997).
80. A. Rupprecht and U. Kaatze, J. Phys. Chem. A **103**, 6485 (1999).
81. K. Menzel, S.Z. Mirzaev, and U. Kaatze, Phys. Rev. E **68**, 011501 (2003).
82. R.B. Gennis. Biomembranes, Molecular Structure and Function (Springer, New York, 1989).
83. W.M. Gelbart, A. Ben-Shaul, and D. Roux. Micelles, Membranes, Microemulsions, and Monolayers (Springer, New York, 1994).
84. Structure and Dynamics of Membranes; From Cells to Vesicles. R. Lipowsky and E. Sackmann, Eds. (Elsevier, Amsterdam, 1995).
85. Structure and Dynamics of Membranes; Generic and Specific Interactions. R. Lipowsky and E. Sackmann, Eds. (Elsevier, Amsterdam, 1995).
86. Biological Membranes – A Molecular Perspective from Computation and Experiment. D. Roux and K.M. Merz, Eds. (Birkhäuser, Boston, MA, 1996).
87. O.G. Mouriston, Chem. Phys. Lipids **57**, 179 (1991).
88. O.G. Mouriston and K. Jorgensen, Chem. Phys. Lipids **73**, 3 (1994).
89. S. Pedersen, K. Jorgensen, T.R. Bakmark, and O.G. Mouriston, Biophys. J. **71**, 554 (1996).
90. S. Halstenberg, W. Schrader, P. Das, J.K. Bhattacharjee, and U. Kaatze, J. Chem. Phys. **118**, 5683 (2003).
91. W. Schrader, S. Halstenberg, R. Behrends, and U. Kaatze, J. Phys. Chem. B **107**, 14457 (2003).
92. J.K. Bhattacharjee and R.A. Ferrell, Phys. Rev. E **56**, 5549 (1997).
93. J. Korlach, P. Schwille, W.W. Webb, and G.W. Feigenson, Proc. Natl. Acad. Sci. USA **96**, 8461 (1991).
94. W. Schrader and U. Kaatze, J. Phys. Chem. B **105**, 6266 (2001).
95. R.L. Smith and E. Oldfield, Science **225**, 280 (1984).
96. R. Behrends and U. Kaatze, J. Phys. Chem. A **104** 3269 (2000).